AGU PUBLICATIONS

Geophysical Research Letters

RESEARCH LETTER
10.1002/2016GL069053

Key Points:
- The presence of nanoparticles alone does not cause weakening without sufficient temperature rise
- Flash heating is the most likely weakening mechanism in experiments on nano-MgO gouges
- Bulk temperature rise and change in contact numbers affect flash weakening on marble bare surface

Supporting Information:
- Supporting Information S1

Correspondence to:
L. Yao,
yaolu_cug@163.com;
luyao@ies.ac.cn

Citation:
Yao, L., S. Ma, A. R. Niemeijer, T. Shimamoto, and J. D. Platt (2016), Is frictional heating needed to cause dramatic weakening of nanoparticle gouge during seismic slip? Insights from friction experiments with variable thermal evolutions, *Geophys. Res. Lett.*, *43*, 6852–6860, doi:10.1002/2016GL069053.

Received 8 APR 2016
Accepted 21 JUN 2016
Accepted article online 23 JUN 2016
Published online 4 JUL 2016

Is frictional heating needed to cause dramatic weakening of nanoparticle gouge during seismic slip? Insights from friction experiments with variable thermal evolutions

Lu Yao[1], Shengli Ma[1], André R. Niemeijer[2], Toshihiko Shimamoto[1], and John D. Platt[3]

[1]State Key Laboratory of Earthquake Dynamics, Institute of Geology, China Earthquake Administration, Beijing, China, [2]Department of Earth Sciences, Utrecht University, Utrecht, Netherlands, [3]Department of Terrestrial Magnetism, Carnegie Institution for Science, Washington, District of Columbia, USA

Abstract To examine whether faults can be lubricated by preexisting and newly formed nanoparticles, we perform high-velocity friction experiments on periclase (MgO) nanoparticles and on bare surfaces of Carrara marble cylinders/slices, respectively. Variable temperature conditions were simulated by using host blocks of different thermal conductivities. When temperature rises are relatively low, we observe high friction in nano-MgO tests and unexpected slip strengthening following initial weakening in marble slice tests, suggesting that the dominant weakening mechanisms are of thermal origin. Solely the rolling of nanoparticles without significant temperature rise is insufficient to cause dynamic fault weakening. For nano-MgO experiments, comprehensive investigations suggest that flash heating is the most likely weakening mechanism. In marble experiments, flash heating controls the unique evolutions of friction, and the competition between bulk temperature rise and wear-induced changes of asperity contact numbers seems to strongly affect the efficiency of flash heating.

1. Introduction

Dynamic weakening of faults plays a key role in facilitating the generation of large earthquakes and rupture propagation. Although dynamic weakening of faults is common, similar for all rock types [e.g., *Di Toro et al*., 2011], the weakening mechanisms and their dominance depend on rock type as well as environmental parameters [*Niemeijer et al*., 2012; *Tullis*, 2015]. Recent work has focused on fault weakening in the presence of nanoscale mineral grains, because these nanoparticles have been widely found within slip zones in various rock deformation experiments, as observed in high-velocity friction tests [e.g., *Han et al*., 2007, 2010; *Reches and Lockner*, 2010], low-velocity friction tests [*Yund et al*., 1990; *Verberne et al*., 2013, 2014], and high-pressure faulting experiments [*Green et al*., 2015]. Besides widely existing in experimentally deformed rock samples, nanoparticles are also abundant in natural fault zones [e.g., *Chester et al*., 2005; *Ma et al*., 2006; *Green et al*., 2015].

Although there are several appealing explanations for the formation of nanoparticles in fault zones [e.g. *Han et al*., 2007; *Sammis and Ben-Zion*, 2008; *Siman-Tov et al*., 2013], their frictional behaviors and the mechanisms by which they may weaken faults remain enigmatic. Based on recent high-velocity rock friction studies, the term "powder lubrication" has been used to describe the fault weakening accompanying the formation of nanoparticles [*Han et al*., 2010, 2011; *Reches and Lockner*, 2010], which is probably partly inspired by many tribological studies in material science [e.g., *Rapoport et al*., 2003; *Wornyoh et al*., 2007]. Recent high-velocity rock friction experiments suggest that nanoparticles can cause dynamic fault weakening by nanograin rolling [*Han et al*., 2011] or by thermally activated diffusion accommodated grain boundary sliding ("superplastic flow") [*De Paola et al*., 2015; *Green et al*., 2015]. However, methodologically speaking, the effectiveness of an individual mechanism cannot be evaluated without controlling temperature conditions during high-velocity sliding, given that several weakening mechanisms may superpose and most of them are thermally activated [*Niemeijer et al*., 2012; *Tullis*, 2015].

In this study, two types of high-velocity friction experiments were conducted, namely, gouge tests using periclase (MgO) nanopowder and rock-on-rock tests using Carrara marble, to investigate whether faults can be lubricated by preexisting and newly formed nanoparticles, respectively. One special and significant

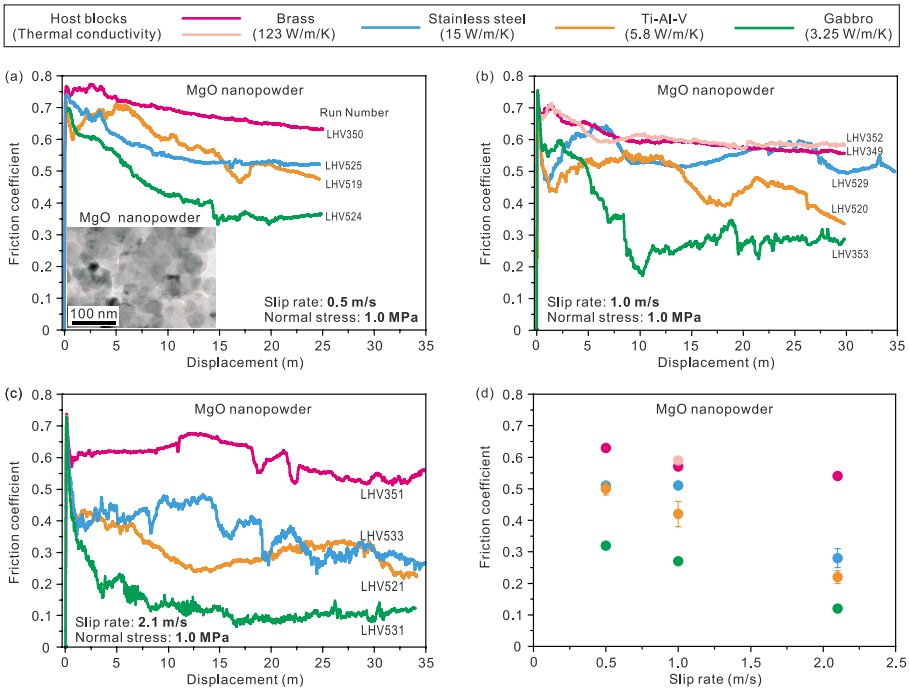

Figure 1. Results of friction experiments performed on magnesium oxide (MgO) nanopowder (<50 nm) at slip rates of 0.5–2.1 m/s under room humidity, with host blocks composed of brass, stainless steel, titanium alloy, and gabbro. (a–c) Friction coefficient versus displacement. (d) Steady state friction coefficient versus slip velocity. A transmission electron microscope image in Figure 1a shows the nano-MgO in their initial state.

design of the experiments is that we use host blocks ("wall rocks") with different thermal conductivities to vary the temperature conditions in the slip zone following *Yao et al*. [2016]. With this strategy, the experiments provide a unique approach to examine dynamic fault-weakening processes in the presence of nanoparticles under varying thermal conditions.

2. Materials and Methods

For easier comparison with previous studies [e.g., *Han et al*., 2010, 2011], MgO nanoparticles are used as the starting material in the gouge experiments. An advantage of using pure nano-MgO is that it avoids complexity arising from comminution and mineral phase changes during the experiments [*Han et al*., 2011]. In addition, MgO nanoparticles can actually be found within shallow fault zones as a decomposition product of dolomite [*De Paola et al*., 2011]. Commercial nano-MgO with an average grain size of ~50 nm is used in the experiments (purity of 99.9%, Aladdin Industrial Inc.; see a transmission electron microscopy image in Figure 1a). The Carrara marble is a typical thermally unstable rock that is able to form nanograins easily in high-velocity friction experiments and has been well studied previously [e.g., *Han et al*., 2007, 2010; *Ree et al*., 2014; *Spagnuolo et al*., 2015], and thus, we use it in our rock-on-rock experiments.

Following *Yao et al*. [2016], we made solid cylindrical host blocks (40 mm in diameter) with brass, stainless steel, titanium alloy, and gabbro, with thermal conductivities of 123, 15, 5.8, and 3.25 W/m/K, respectively. For the nano-MgO experiments, the simulated gouge (2.5 g and ~1.5 mm thick for each test) is sandwiched by a pair of host blocks, surrounded by a Teflon sleeve to prevent loss of gouge during slip. For the experiments on Carrara marble (thermal conductivity: 2.41 W/m/K [*Čermák and Rybach*, 1982]), besides using the marble cylinders directly, we also performed a few experiments on thin circular marble slices that were bonded to the above-mentioned three kinds of metal host blocks using a high thermally conductive epoxy adhesive (1.38 W/m/K; OB-200, Omega Engineering, Inc.). The marble slices were carefully machined to a thickness of 0.5 ± 0.05 mm (Figures 2 and S1; see details of sample preparation in supporting information). The experiments were performed with a rotary-shear low- to high-velocity frictional testing machine [*Ma et al*., 2014]. All the experiments were conducted at constant velocities (0.5–2.1 m/s) under a normal stress of 1.0 MPa and at room humidity.

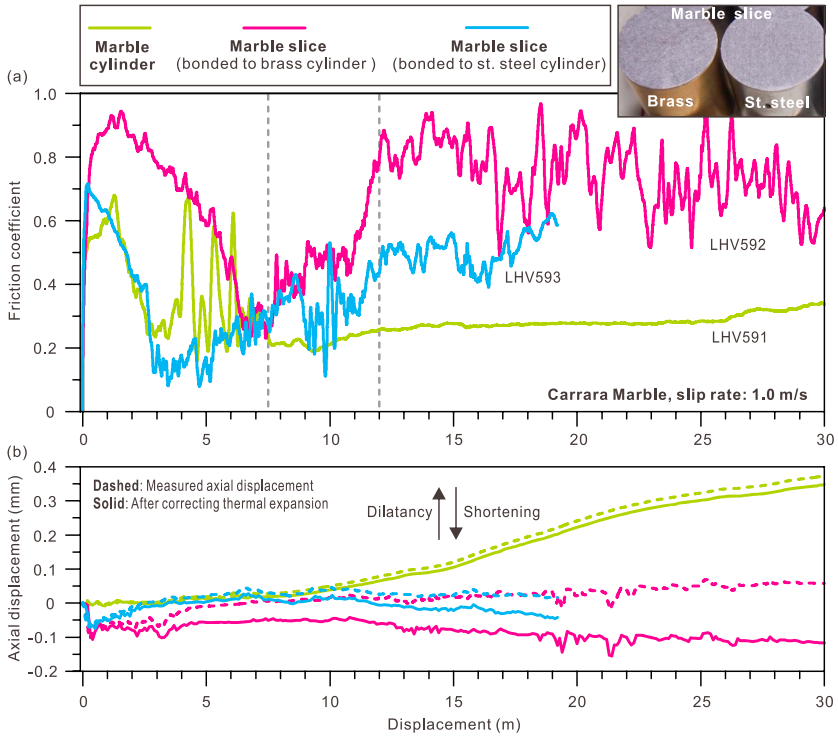

Figure 2. Evolution of (a) friction coefficient and (b) axial displacement with shear displacement in constant velocity (1.0 m/s) experiments performed on Carrara marble cylinders and slices that are bonded to brass and stainless steel host blocks (see a photograph in the upper right corner; the gray color of the marble is due to the underlying black-colored epoxy). Solid and dashed lines in Figure 2b denote axial displacement data with and without correcting for thermal expansion of specimens, respectively.

3. Results

3.1. Frictional Behavior

Thirteen experiments were performed on the MgO nanopowder at slip rates of 0.5, 1.0, and 2.1 m/s with the four kinds of host blocks. Figures 1a–1c show the evolution of friction coefficient with displacement in these tests. The peak friction coefficients, μ_p, in all cases are about 0.70–0.80, but the postpeak friction coefficients show clear negative correlation with thermal conductivities of host blocks λ_h, i.e., the lower λ_h, the more and quicker weakening occurs. The steady state friction coefficient μ_{ss} was determined by fitting the curves with Mizoguchi's equation ([*Mizoguchi et al.*, 2007]) for exponential-decay type data or by averaging the friction coefficient near the end of tests. The μ_{ss} in all the experiments are plotted against slip rate V in Figure 1d. We observe velocity-weakening trends in all cases, but the overall level of μ_{ss} is highly variable. Note that μ_{ss} remains high (~0.54) even at $V = 2.1$ m/s with brass host blocks.

In Figures 2a and 2b, we plot the evolution of friction coefficient and axial displacement with shear displacement in the experiments ($V = 1.0$ m/s) performed on Carrara marble cylinder (LHV591) and on the marble slices that were bonded to brass (LHV592) and stainless steel (LHV593) host blocks. Because the failure temperature of the epoxy adhesive is about 260°C, the test performed with titanium alloy blocks failed (not shown here) and the test with stainless steel lost some sample in the later stage. The three experiments shown in Figure 2a exhibit dramatic weakening soon after a somewhat variable peak friction ($\mu_p = 0.68$–0.94), then the friction evolves in different ways. For the marble cylinder test (LHV591), a steady state friction was achieved with μ_{ss} of 0.27. In contrast, the marble slice tests exhibit slip strengthening at displacements of 7–12 m after which a steady state friction was achieved with μ_{ss} of 0.80 ± 0.10 (LHV592; brass host blocks) and 0.51 ± 0.05 (LHV593; steel blocks), respectively. The measured changes of axial displacement in Figure 2b (dashed lines) may include contributions from wear of marble surfaces, material extrusion, and thermal expansion. The corrected data, after subtracting thermal expansion (solid lines; see details in supporting information), reveal that only small amount of dilatancy (50–90 μm) occurred in the two marble

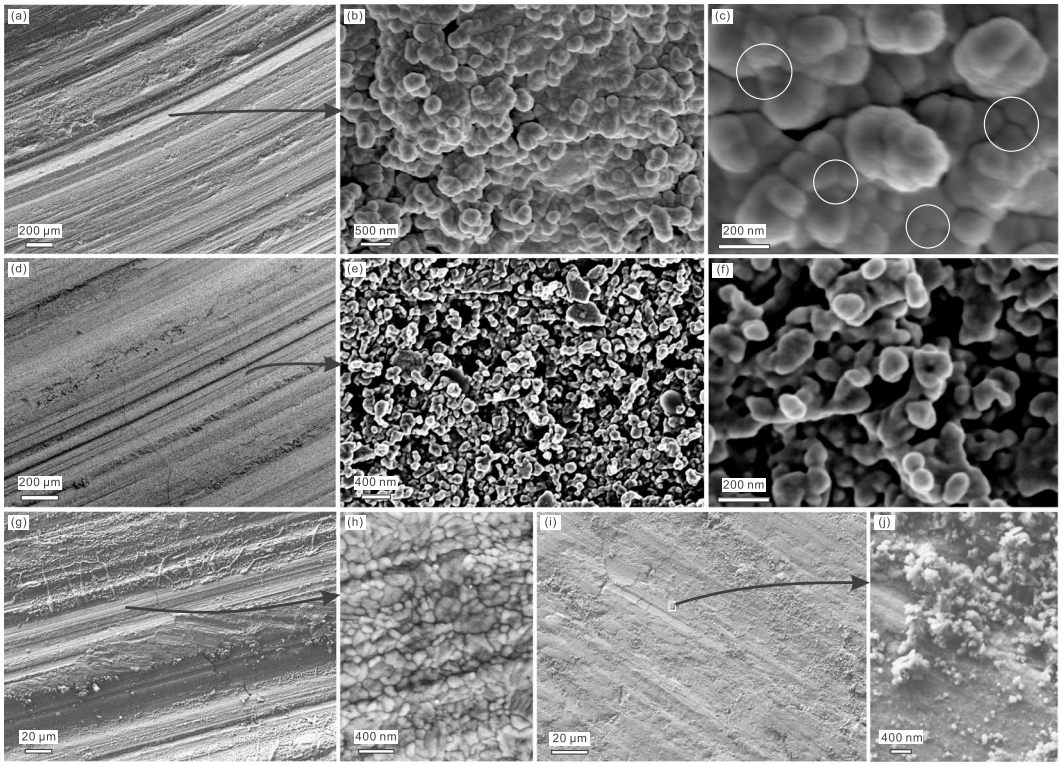

Figure 3. Secondary electron images of slip surfaces recovered after high-velocity friction experiments. Figures 3a–3c and 3d–3f are images for experiments conducted on MgO nanopowder with gabbro (run LHV531) and brass (LHV351) host blocks, respectively. Figures 3g and 3h and 3i and 3j are for experiments on Carrara marble cylinders (LHV591) and brass-bonded marble slices (LHV592), respectively.

slice tests (at displacements of ~3.5–11 m for test LHV592 and 0.5–10 m for test LHV 593), in contrast to much greater dilatancy (~370 μm) after the initial weakening in the marble cylinder test (LHV591).

3.2. Microstructures

Small pieces of the slip surfaces developed in nano-MgO experiments were collected after removing the rotary host blocks. In Figures 3a–3c and 3d–3f, we present secondary electron images of the slip surfaces developed in the tests ($V = 2.1$ m/s) performed with gabbro (LHV531) and brass (LHV351) blocks, respectively. In both cases, the slip surfaces show grooves oriented parallel to the slip direction (Figures 3a and 3d). Higher magnification images reveal the slip surfaces consisting of nanocrystalline MgO (Figure 3b and 3e). However, the slip surface developed with gabbro host blocks (Figure 3b) comprises denser particle aggregates than that with brass blocks (Figure 3e). Furthermore, the nano-MgO sheared with gabbro shows polygonal nanostructures and straight grain boundaries with 120° triple junction contacts between the grains (Figure 3c; see examples in the white circles). By comparing the size of nano-MgO before (~50 nm; Figures 1a) and after experiments (Figures 3b and 3c and 3e and 3f), grain growth after the experiments can be observed, especially in the case of gabbro host blocks (up to ~300 nm; Figure 3c).

Figures 3g and 3h and 3i and 3j show slip surfaces developed in the tests performed on the marble cylinders (LHV591) and on the brass-bonded marble slices (LHV592), respectively. For the marble cylinder test, energy dispersive X-ray spectrometry analysis indicate that the grooved portions of the slip surface (Figure 3g) are mainly lime (CaO) aggregates as seen at higher magnification in Figure 3h at nanoscale, while the brighter spots and ribbons near or covering the grooves are hydrated lime or calcium carbonate probably formed from post-slip reactions of CaO in air (the weight ratio of Ca to O is used to roughly distinguish these). For the brass-bonded marble slice test, CaO is minimally detected on the slip surface except within some tiny grooves. The abrasion is not as serious as that in the marble cylinder test, but nanoparticles are still widely distributed on the slip surface (Figures 3i and 3j).

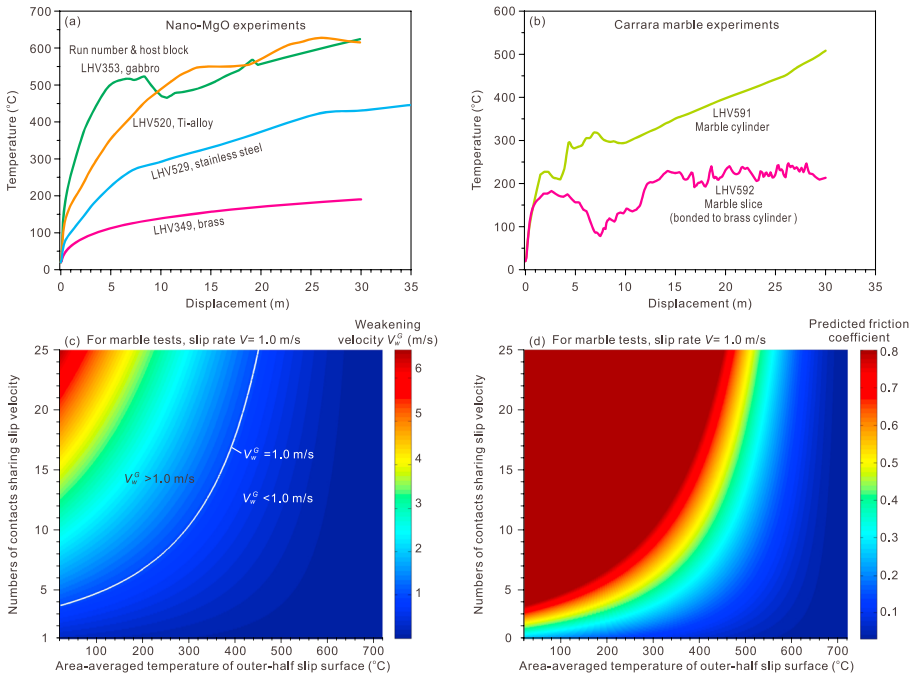

Figure 4. Calculated area-averaged temperature of the outer-half slip surface versus displacement for selected experiments on (a) MgO nanopowder and (b) Carrara marble, as shown in Figures 1b and 2a, respectively. (c and d) The characteristic weakening velocity V_w^G and the predicted friction coefficient of the marble (from bare surface to wear-induced gouge grains) as a function of the number of contacts sharing the total slip velocity N_{con} and the fault temperature T_f.

3.3. Temperature Estimation

The temperature rise in the sample assembly during the experiments was estimated using a finite-element method implemented in the COMSOL Multiphysics software, following similar procedures reported previously [e.g., *Kitajima et al*., 2010; *Han et al*., 2011; *Yao et al*., 2013] (see details of the model and material properties in supporting information). The area-averaged temperature of the outer-half slip surface was selected as representative of the overall fault temperature T_f. Figure 4a shows the evolution of T_f during the nano-MgO experiments performed with the four types of host blocks at $V = 1.0$ m/s and $\sigma_n = 1.0$ MPa. The rates of temperature rise are highly variable in these tests, as are the differences in final temperature (up to 400–450°C). Figure 4b shows the evolution of T_f in the experiments performed on the marble cylinders and brass-bonded marble slices. The T_f in the former case continues to increase towards a final temperature of ~500°C; in contrast, the T_f evolution in the latter case is more sensitive to the evolution of shear stress and finally stabilizes at a temperature of ~250°C.

4. Discussion

4.1. Dynamic Weakening Mechanisms of MgO Nanopowder

The diverse frictional behaviors of MgO nanopowder observed in the experiments with host blocks of different thermal conductivities (Figure 1) are quite similar to those reported recently by *Yao et al*. [2016], where the same kinds of host blocks were used in experiments performed on an illite-quartz gouge and pure quartz gouge. *Yao et al*. [2016] questioned the effectiveness of powder lubrication based on the observation of high friction in sheared gouges with nanoparticles present but with limited temperature rise. Our experiments on MgO nanopowder with brass blocks provide strong evidence to support this earlier result because the starting material consists of 100% nanoparticles. The use of dry MgO nanopowder avoids the complexity arising from potential phase changes of minerals, comminution, thermochemical pressurization, and frictional melting. By examining the dynamic fault-weakening mechanisms as summarized in *Tullis* [2015], we argue that the only remaining candidate mechanisms, which have to be thermal in origin or thermally enhanced, are flash heating and rapid superplastic deformation.

Flash heating is an important dynamic fault-weakening mechanism with wide applicability [e.g., *Rice*, 2006; *Goldsby and Tullis*, 2011]. However, *Han et al*. [2011] estimated flash temperature on the contacts between MgO nanograins using equations derived by *Archard* [1959] and concluded that flash heating is not effective for nano-MgO gouges as the calculated flash temperature is quite low (<53.3°C). However, Archard's model of flash temperature considered a one-dimensional heat conduction problem for a single circular asperity moving over a large flat surface [*Archard*, 1959], which is modeled as a semi-infinite half-space. The assumption of a semi-infinite plane is justified by showing that the size of the thermal boundary layer that forms at the slipping contact is much smaller than the distance between neighboring contacts. However, while this assumption is valid for bare rock surfaces or gouges with large grains, for frictional slip on nanoscale contacts within a volume of nanograins, the assumption of an asperity moving over a semi-infinite solid may break down and heat generated at one contact may be able to diffuse to a neighboring contact within a contact lifetime. Thus, it is unsuitable to use the existing models in *Archard* [1959] and *Rice* [2006] to analyze the flash-weakening process within a volume of nanograins. Furthermore, in the small grain size limit, heat generated by deformation within grains, such as the recently hypothesized fast dislocation avalanches [*Armstrong and Elban*, 1989; *Spagnuolo et al*., 2015], has time to diffuse to nearby contacts, which raises the contact temperature and allows flash heating to be triggered at slip rates below the critical weakening velocity. Given the above-mentioned limitations and uncertainties associated with current flash heating models, flash heating cannot be eliminated as a potential weakening mechanism for nano-MgO gouges. In fact, we managed to fit the data produced in test LHV531 well using the flash heating model from *Yao et al*. [2016] and parameter values of $T_w = 646$°C and $V_{w\_ini} = 2.59$ m/s (T_w and V_{w_ini} are the weakening temperature and the initial weakening velocity, respectively). However, this weakening temperature appears too low for melting of MgO, so either significant weakening can occur below the melting temperature, as discussed in *Rice* [2006] and *Beeler et al*. [2008], or two free parameters are enough to describe any high-velocity friction experiment and we have overfit our data. Unfortunately, little is currently known about the thermodynamic processes of nanoparticles undergoing rapid frictional heating and extremely large deformation associated with the high-velocity sliding, which makes it difficult to know the concrete weakening process and the weakening temperature on the MgO nanocontacts.

The MgO nanopowder deformed with gabbro host blocks show polygonal textures with triple junctions between equant nanograins (Figures 3b and 3c). These are diagnostic microstructures of grain boundary sliding accommodated by grain size sensitive diffusion ("superplastic flow") [*Ranalli*, 1995]. These observations seem to accord with previous studies on dense MgO nanoceramics, in which superplastic behavior occurred at temperatures as low as ~700°C [*Domínguez-Rodríguez et al*., 2007, 2010]. However, in terms of the flow stress of 200–650 MPa, activation energy of 200 kJ/mol and stress exponent of 2 reported in *Domínguez-Rodríguez et al*. [2007, 2010], the flow stress is many orders of magnitude too high to explain the observed friction and the activation energy is much too high to explain why the friction coefficient decreases by only a factor of three while the temperature increases by ~500°C. Furthermore, the superplastic flow may encounter problems in explaining the pressure dependence of shear resistance during high-velocity sliding. Therefore, we exclude the superplasticity of bulk MgO nanograins as a possible weakening mechanism. Then it is unclear how the observed polygonal textures may form although the sintering is probably one of the processes involved. This is mainly because little is currently known about the possible plastic deformations that may occur at the contact scale especially for nanograins. However, in this case the discussion of plasticity reduces to understanding the contact scale weakening mechanisms that underpin flash weakening. In conclusion, the above discussion justifies excluding superplasticity of bulk MgO nanograins from the possible candidate mechanisms that could explain the temperature-dependent weakening, leaving flash heating as the only remaining mechanism that could explain the dynamic weakening observed in the nano-MgO experiments.

4.2. Cause of Unique Frictional Behavior in Carrara Marble Tests

In Figure 2a, the significant differences in final steady state friction for the three marble experiments with different host rock conductivities suggest that temperature-dependent weakening mechanisms control the overall weakening processes. However, the rapid weakening followed by sharp strengthening observed in the two marble slice tests remains enigmatic, especially considering that the slip velocity of 1.0 m/s is larger than the characteristic flash-weakening velocity of bare marble surface (~0.27 m/s; Table S3). In our

judgement, the most plausible interpretation for the unique frictional behavior is the variation in flash heating efficiency caused by the evolution of asperity contact numbers and fault temperature as discussed below.

Platt et al. [2014] presented an updated flash heating model applicable to a gouge layer by considering that the total slip rate is shared between a uniformly distributed set of contacts. Compared with the classic model of flash heating on bare surfaces [*Rice*, 2006], the theoretical analysis in *Rempel* [2006] and *Platt et al*. [2014] leads to

$$V_w^G = N_{\mathrm{con}} \cdot V_w^{BS} \tag{1}$$

where V_w^G and V_w^{BS} are characteristic weakening velocities of a gouge layer and a bare surface for the same rock samples, respectively, and N_{con} is the number of asperity contacts sharing the total slip velocity across the gouge layer. The model thus predicts that flash heating is much less efficient in gouge than for bare surface at the same conditions. Our experiments on Carrara marble started from bare surfaces, but wear occurred and shear deformation became distributed through the ensuing gouge immediately after slip initiation. From equation (1), it is clear that creation of a gouge causes an increase in V_w^G through an increase in N_{con}, assuming that deformation does not localize significantly within the newly created gouge. At the same time, the temperature rise driven by frictional heating lowers V_w^G, as shown in *Platt et al*. [2014] with some experimental support [*Proctor et al*., 2014; *Yao et al*., 2016]. Thus, the increase in N_{con} with gouge creation competes with the temperature rise from frictional heating, leading to a change in the efficiency of flash heating. In practice, it is not easy to estimate the evolution of N_{con} in our experiments because N_{con} is not simply proportional to gouge thickness, let alone the complexity arising from the extrusion of material.

In recognition of the latter issues, the observed frictional behavior is analyzed semiquantitatively here. Using the equation for V_w^{BS} [*Rice*, 2006; *Beeler et al*., 2008] and considering the roles of N_{con} and T_f [*Platt et al*., 2014], the V_w^G of the marble as a function of N_{con} and T_f is plotted in Figure 4c (see material parameters in Table S3 and more details in supporting information). The white line in the figure denotes the V_w^G equal to V of 1.0 m/s as used in the experiments and thus demarcates the N_{con}-T_f conditions at which flash weakening is effective ($V_w^G < 1.0$ m/s) or ineffective ($V_w^G > 1.0$ m/s). Using the equations from *Rice* [2006] and *Beeler et al*. [2008] for friction coefficient as a function of slip rate, we predict how changes in the critical weakening velocity cause the macroscopic friction coefficient to change with N_{con} and T_f (Figure 4d).

In the experiments on the marble cylinders and brass-bonded marble slices, the temperature evolutions become very different after experiments ran for 3–4 s (Figure 4b), because the conductivity of the marble cylinder is much lower than that of the marble slice plus brass. Linking the results in Figures 4b–4d with the frictional behaviors in the three marble tests (Figure 2a), we deduce that the V_w^G over the first several meters displacements in the tests is probably lower than the slip velocity (1.0 m/s) due to elevated T_f and small N_{con} (i.e., not enough gouge has accumulated yet), leading to dramatic weakening for all the three cases. However, with gouge continuously being created, it becomes critical for the effectiveness of flash weakening whether the effects of T_f can compensate for the opposing effects of N_{con}. From the frictional data of the two marble slice tests, it is observed that the strengthening starts earlier for the steel host blocks case, which coincides with an earlier start of dilation than for the brass blocks case (Figure 2b), possibly reflecting the effects of N_{con} on the efficiency of flash heating. To meet $V_w^G < 1.0$ m/s, the brass-bonded marble slice test allows N_{con} less than 8 with T_f of ~250°C, while the marble cylinder test allows N_{con} up to about 40 with T_f of ~500°C towards the end of the test (Figures 4b and 4c). These differences influence the efficiency of flash heating in these tests, causing different frictional behaviors after the initial onset of weakening. Moreover, in the later stage of the marble cylinder test, other weakening mechanisms such as thermochemical pressurization may be also involved, which assists in maintaining low friction.

5. Conclusions

Our study demonstrates that a preexisting layer of nanopowder cannot lubricate faults effectively if the fault zone temperature rise is suppressed. Since there are currently no proposed mechanisms that would make the rolling of nanoparticles depend on temperature, our experiments suggest that nanoparticle rolling cannot cause dynamic fault-weakening efficiently. As the dominant weakening mechanisms are of thermal origin in dry nano-MgO experiments, flash heating and superplastic flow are the only remaining candidate

mechanisms. However, given the high flow stress and activation energy of bulk MgO nanograins at our experimental conditions, superplastic flow cannot explain the observed weakening. Thus, flash heating is the most likely weakening mechanism in the nano-MgO experiments. Experiments conducted on Carrara marble slices and cylinders at variable temperature conditions reveal rapid slip weakening followed by diverse friction evolutions with different final steady state strength, regardless of the widely distributed presence of nanograins on the slip surfaces in all the cases. The unexpected slip strengthening following initial weakening observed in the marble slice tests is reconciled with an updated flash heating model [*Platt et al*., 2014] that considers the competing roles of gouge formation and temperature. Using this model, our analysis illustrates that the efficiency of flash weakening on bare rock surfaces can be changed with progressive slip by a competition between the effects of bulk temperature rise and wear-induced variations in contact numbers accommodating slip.

Acknowledgments

We sincerely thank Raehee Han, an anonymous reviewer, and the Associate Editor Ake Fagereng for careful and constructive reviews. We also thank B.A. Verberne for sharing Carrara marble samples with us and L. Zhang and J. Chen for the helpful discussion. Financial support for this study was partially provided by the State Key Laboratory of Earthquake Dynamics (LED2014A06) and the National Natural Science Foundation of China (41404143). A.R. Niemeijer was funded by European Research Council starting grant SEISMIC (335915) and by the Netherlands Organization for Scientific Research (NWO) through a VIDI grant (854.12.011). J.D. Platt was funded by a postdoctoral fellowship from the Department of Terrestrial Magnetism at the Carnegie Institution for Science (Washington, DC, USA). The authors have no financial conflict of interest. Data underlying the present paper are available upon a request to the corresponding author (L. Yao).

References

Archard, J. F. (1959), The temperature of rubbing surfaces, *Wear*, *2*(6), 438–455.

Armstrong, R. W., and W. L. Elban (1989), Temperature rise at a dislocation pile-up breakthrough, *Mater. Sci. Eng., A*, *122*, L1–L3.

Beeler, N. M., T. E. Tullis, and D. L. Goldsby (2008), Constitutive relationships and physical basis of fault strength due to flash heating, *J. Geophys. Res.*, *113*, B01401, doi:10.1029/2007JB004988.

Čermák, V., and L. Rybach (1982), Thermal conductivity and specific heat of minerals and rocks, in *Landolt-Bornstein Zahlenwerte and Funktionen aus Naturwissenschaften und Technik, Neue Serie, Physikalische Eigenschaften der Gesteine (V/1a)*, edited by G. Angeneister, pp. 305–343, Springer, New York.

Chester, J. S., F. M. Chester, and A. K. Kronenberg (2005), Fracture surface energy of the Punchbowl fault, San Andreas system, *Nature*, *437*(7055), 133–136, doi:10.1038/nature03942.

De Paola, N., T. Hirose, T. Mitchell, G. Di Toro, C. Viti, and T. Shimamoto (2011), Fault lubrication and earthquake propagation in thermally unstable rocks, *Geology*, *39*(1), 35–38, doi:10.1130/g31398.1.

De Paola, N., R. E. Holdsworth, C. Viti, C. Collettini, and R. Bullock (2015), Can grain size sensitive flow lubricate faults during the initial stages of earthquake propagation?, *Earth Planet. Sci. Lett.*, *431*, 48–58, doi:10.1016/j.epsl.2015.09.002.

Di Toro, G., R. Han, T. Hirose, N. De Paola, S. Nielsen, K. Mizoguchi, F. Ferri, M. Cocco, and T. Shimamoto (2011), Fault lubrication during earthquakes, *Nature*, *471*(7339), 494–498, doi:10.1038/nature09838.

Domínguez-Rodríguez, A., D. Gómez-García, E. Zapata-Solvas, J. Z. Shen, and R. Chaim (2007), Making ceramics ductile at low homologous temperatures, *Scr. Mater.*, *56*(2), 89–91, doi:10.1016/j.scriptamat.2006.09.024.

Domínguez-Rodríguez, A., D. Gómez-García, M. Castillo-Rodríguez, E. Zapata-Solvas, and R. Chaim (2010), Superplasticity in nanocrystalline ceramics: Pure grain boundary phenomena or not?, *Int. J. Mater. Res.*, *101*(10), 1215–1221.

Goldsby, D. L., and T. E. Tullis (2011), Flash heating leads to low frictional strength of crustal rocks at earthquake slip rates, *Science*, *334*(6053), 216–218, doi:10.1126/science.1207902.

Green, H. W., F. Shi, K. Bozhilov, G. Xia, and Z. Reches (2015), Phase transformation and nanometric flow cause extreme weakening during fault slip, *Nat. Geosci.*, *8*(6), 484–489, doi:10.1038/ngeo2436.

Han, R., T. Shimamoto, T. Hirose, J.-H. Ree, and J.-i. Ando (2007), Ultralow friction of carbonate faults caused by thermal decomposition, *Science*, *316*(5826), 878–881, doi:10.1126/science.1139763.

Han, R., T. Hirose, and T. Shimamoto (2010), Strong velocity weakening and powder lubrication of simulated carbonate faults at seismic slip rates, *J. Geophys. Res.*, *115*, B03412, doi:10.1029/2008JB006136.

Han, R., T. Hirose, T. Shimamoto, Y. Lee, and J.-i. Ando (2011), Granular nanoparticles lubricate faults during seismic slip, *Geology*, *39*(6), 599–602, doi:10.1130/g31842.1.

Kitajima, H., J. S. Chester, F. M. Chester, and T. Shimamoto (2010), High-speed friction of disaggregated ultracataclasite in rotary shear: Characterization of frictional heating, mechanical behavior, and microstructure evolution, *J. Geophys. Res.*, *115*, B08408, doi:10.1029/2009JB007038.

Ma, K.-F., et al. (2006), Slip zone and energetics of a large earthquake from the Taiwan Chelungpu-fault Drilling Project, *Nature*, *444*(7118), 473–476, doi:10.1038/nature05253.

Ma, S., T. Shimamoto, L. Yao, T. Togo, and H. Kitajima (2014), A rotary-shear low to high-velocity friction apparatus in Beijing to study rock friction at plate to seismic slip rates, *Earthquake Sci.*, *27*, 469–497, doi:10.1007/s11589-014-0097-5.

Mizoguchi, K., T. Hirose, T. Shimamoto, and E. Fukuyama (2007), Reconstruction of seismic faulting by high-velocity friction experiments: An example of the 1995 Kobe earthquake, *Geophys. Res. Lett.*, *34*, L01308, doi:10.1029/2006GL027931.

Niemeijer, A., G. Di Toro, W. A. Griffith, A. Bistacchi, S. A. Smith, and S. Nielsen (2012), Inferring earthquake physics and chemistry using an integrated field and laboratory approach, *J. Struct. Geol.*, *39*, 2–36, doi:10.1016/j.jsg.2012.02.018.

Platt, J. D., B. P. Proctor, T. M. Mitchell, G. Hirth, D. L. Goldsby, G. Di Toro, N. M. Beeler, and T. E. Tullis (2014), The role of gouge and temperature on flash heating and its hysteresis, Abstract S11C–4360 presented at 2014 Fall Meeting, AGU, San Francisco, Calif., 15–19 Dec.

Proctor, B. P., T. M. Mitchell, G. Hirth, D. Goldsby, F. Zorzi, J. D. Platt, and G. Di Toro (2014), Dynamic weakening of serpentinite gouges and bare surfaces at seismic slip rates, *J. Geophys. Res. Solid Earth*, *119*, 8107–8131, doi:10.1002/2014JB011057.

Ranalli, G. (1995), *Rheology of the Earth*, 2nd ed., Chapman and Hall, New York.

Rapoport, L., V. Leshchinsky, M. Lvovsky, I. Lapsker, Y. Volovik, Y. Feldman, R. Popovitz-Biro, and R. Tenne (2003), Superior tribological properties of powder materials with solid lubricant nanoparticles, *Wear*, *255*(7–12), 794–800, doi:10.1016/S0043-1648(03)00285-0.

Reches, Z. e., and D. A. Lockner (2010), Fault weakening and earthquake instability by powder lubrication, *Nature*, *467*(7314), 452–455, doi:10.1038/nature09348.

Ree, J.-H., J.-i. Ando, R. Han, and T. Shimamoto (2014), Coseismic microstructures of experimental fault zones in Carrara marble, *J. Struct. Geol.*, *66*, 75–83, doi:10.1016/j.jsg.2014.05.012.

Rempel, A. (2006), The effects of flash-weakening and damage on the evolution of fault strength and temperature, in *Radiated Energy and the Physics of Earthquake Faulting*, *Geophys. Monogr. Ser.*, vol. 170, edited by R. Abercrombie et al., pp. 263–270, AGU, Washington, D. C., doi:10.1029/170GM26.

Rice, J. R. (2006), Heating and weakening of faults during earthquake slip, *J. Geophys. Res.*, *111* B05311, doi:10.1029/2005JB004006.
Sammis, C. G., and Y. Ben-Zion (2008), Mechanics of grain-size reduction in fault zones, *J. Geophys. Res.*, *113*, B02306, doi:10.1029/2006JB004892.
Siman-Tov, S., E. Aharonov, A. Sagy, and S. Emmanuel (2013), Nanograins form carbonate fault mirrors, *Geology*, *41*(6), 703–706, doi:10.1130/g34087.1.
Spagnuolo, E., O. Plümper, M. Violay, A. Cavallo, and G. Di Toro (2015), Fast-moving dislocations trigger flash weakening in carbonate-bearing faults during earthquakes, *Sci. Rep.*, *5*, 16,112, doi:10.1038/srep16112.
Tullis, T. E. (2015), Mechanisms for friction of rock at earthquake slip rates, in *Treatise on Geophysics*, 2nd ed., edited by G. Schubert, pp. 139–159, Elsevier, Oxford.
Verberne, B. A., J. H. P. de Bresser, A. R. Niemeijer, C. J. Spiers, D. A. M. de Winter, and O. Plümper (2013), Nanocrystalline slip zones in calcite fault gouge show intense crystallographic preferred orientation: Crystal plasticity at sub-seismic slip rates at 18–150 °C, *Geology*, *41*(8), 863–866, doi:10.1130/G34279.1.
Verberne, B. A., O. Plümper, D. A. Matthijs de Winter, and C. J. Spiers (2014), Superplastic nanofibrous slip zones control seismogenic fault friction, *Science*, *346*(6215), 1342–1344, doi:10.1126/science.1259003.
Wornyoh, E. Y. A., V. K. Jasti, and C. F. Higgs III (2007), A review of Dry particulate lubrication: Powder and granular materials, *ASME J. Tribol.*, *129*(2), 438–449, doi:10.1115/1.2647859.
Yao, L., T. Shimamoto, S. Ma, R. Han, and K. Mizoguchi (2013), Rapid postseismic strength recovery of Pingxi fault gouge from the Longmenshan fault system: Experiments and implications for the mechanisms of high-velocity weakening of faults, *J. Geophys. Res. Solid Earth*, *118*, 4547–4563, doi:10.1002/jgrb.50308.
Yao, L., S. Ma, J. D. Platt, A. R. Niemeijer, and T. Shimamoto (2016), The crucial role of temperature in high-velocity weakening of faults: Experiments on gouge using host blocks with different thermal conductivities, *Geology*, *44*(1), 63–66, doi:10.1130/g37310.1.
Yund, R. A., M. L. Blanpied, T. E. Tullis, and J. D. Weeks (1990), Amorphous material in high strain experimental fault gouges, *J. Geophys. Res.*, *95*(B10), 15,589–15,602, doi:10.1029/JB095iB10p15589.